

# PROCEEDINGS OF SPIE

[SPIDigitalLibrary.org/conference-proceedings-of-spie](https://SPIDigitalLibrary.org/conference-proceedings-of-spie)

## Evaluating the effects of distinct water saturation states on the light penetration depths of sand-textured soils

Baranoski, Gladimir V., Iwanchyshyn, Mark, Kimmel, Bradley, Varsa, Petri, Van Leeuwen, Spencer

Gladimir V. G. Baranoski, Mark Iwanchyshyn, Bradley W. Kimmel, Petri M. Varsa, Spencer R. Van Leeuwen, "Evaluating the effects of distinct water saturation states on the light penetration depths of sand-textured soils," Proc. SPIE 11856, Remote Sensing for Agriculture, Ecosystems, and Hydrology XXIII, 118560U (12 September 2021); doi: 10.1117/12.2592956

**SPIE.**

Event: SPIE Remote Sensing, 2021, Online Only

# Evaluating the Effects of Distinct Water Saturation States on the Light Penetration Depths of Sand-Textured Soils

Gladimir V. G. Baranoski, Mark Iwanchyshyn, Bradley W. Kimmel,  
Petri M. Varsa and Spencer R. Van Leeuwen

University of Waterloo, David R. Cheriton School of Computer Science, Natural Phenomena  
Simulation Group, 200 University Avenue West, Waterloo, Ontario, N2L 3G1, Canada

## ABSTRACT

The high-fidelity estimation of the light penetration depths of dry and wet sand-textured soils is of considerable interest for applied remote sensing and geoscience research initiatives involving a wide range of landscapes, from deserts and arable fields to coastal habitats. These initiatives include the restoration of vegetation in arid regions and the mitigation of weed dissemination in agricultural areas covered by wind-transported layers of these soils. Similarly, the remote detection and analysis of hyperspectral signatures from subsurface targets located in sandy landscapes also requires a sound understanding about the light penetration properties of the covering particulate materials under dry and wet conditions. Despite their relevance, however, there is a noticeable lack of data on the light penetration depths of sand-textured soils, notably accounting for their sensitivity to distinct patterns of water presence, either in their pore space or forming films around their grains. In this work, we aim to make inroads, both qualitatively and quantitatively, toward the understanding of key aspects associated with these interconnected processes. In order to achieve this goal without being constrained by laboratory and logistics limitations, we performed an array of controlled *in silico* experiments to systematically evaluate the effects of distinct water saturation states on the light penetration depths of representative samples of sand-textured soils. Our investigation was centered at the 400 to 1000 nm spectral domain, relevant for studies involving the mineralogy and morphology of natural sands, and it was carried out employing a first-principles simulation framework supported by actual measured data. By advancing the current knowledge in this area, our findings are expected to contribute to the development of new technologies aimed at the cost-effective monitoring and management of landscapes covered by natural sand deposits, and at the acquisition of more precise data on fundamental biophysical phenomena (e.g., seed germination) with a direct impact on crop yield and the recovery of ecosystems affected by the expansion of arid terrains.

**Keywords:** soil, natural sands, light penetration depth, water saturation, hyperspectral signatures, iron oxides, remote sensing, geoscience, ecology, precision agriculture

## 1. INTRODUCTION

Sand-textured soils, commonly referred to as natural sands, make up for more than 35% of the planet's land surface.<sup>1,2</sup> Their presence tends to become even more widespread as aridification and desertification processes elicited by climate change and human activities continue to have a negative impact on ecosystems around the globe, notably on drylands.<sup>2,3</sup> Accordingly, the use of hyperspectral technologies to monitor and analyze these ubiquitous particulate materials represents one of the focal points of applied research initiatives in several fields, from remote sensing and geoscience to ecology and agriculture.

These initiatives include, for instance, the restoration of vegetation in arid regions<sup>4</sup> and the mitigation of weed dissemination in agricultural areas,<sup>5</sup> particularly those covered by layers of these soils that have been transported by extreme aeolian events like sand and dust storms.<sup>6,7</sup> The success of these initiatives, in turn, is associated with the reliable assessment, both remotely and *in situ*, of interconnected abiotic factors, notably light penetration and water presence in these soils,<sup>8,9</sup> affecting the germination and development of plant seedlings.<sup>10,11</sup> Similarly, the detection and analysis of hyperspectral signatures from subsurface targets located in sandy landscapes also requires reliable information about the light penetration depth (LPD) of these areas,<sup>12</sup> under dry and wet conditions. The quantity is normally defined as the depth in which the incident light is reduced by  $\geq 99\%$ ,

yielding transmittance readings  $\leq 1\%$ .<sup>12,13</sup> It also represents a key piece of data for geophysical studies relying on optical dating<sup>14</sup> to predict changes in natural sand deposits,<sup>15</sup> particularly those found in regions more vulnerable to environmental changes like coasts and deltas.

Light penetration in sand-textured soils can be directly measured (in terms of transmittance) using a spectrophotometer, or indirectly gauged using the germination of light-sensitive seeds or the presence of growing algae as bioindicators.<sup>8</sup> However, despite relevant efforts in these areas,<sup>8,9</sup> there is only a scarce number of transmittance datasets for naturally-occurring sand-textured soils available in the literature. Furthermore, besides covering a relatively limited variety of these soils, these datasets have their generalization often hindered by experimental and logistics constraints. For example, techniques employed to obtain *in situ* samples of sand deposits often involve the physical handling of these samples. This, in turn, can result in grain breakage and pore space disturbance problems (*e.g.*, grain-to-grain rearrangement),<sup>16–18</sup> which can alter the samples' core structure and affect transmittance measurements.

On the other hand, samples artificially prepared and mixed in the laboratory<sup>19,20</sup> generally lack key morphological features of natural sands (*e.g.*, the complex size distribution patterns of their constituent grains<sup>21</sup>). In addition, often samples with relatively uncommon mineralogical characteristics, such as absence of mineral impurities,<sup>22</sup> are used in the experiments to facilitate the detection of transmittance signals. This jeopardizes the use of these datasets in high-fidelity estimations of natural sands' LPD since these impurities have a significant impact on the attenuation of the propagated light.<sup>23</sup> In the case of models used in conjunction with transmittance measurement initiatives, they usually do not explicitly incorporate in their formulations the particulate nature of natural sands,<sup>12,19,22,24</sup> which restricts their predictive capabilities.

The radiometric responses of sand-textured soils can be significantly affected by their water content.<sup>25,26</sup> In fact, the retrieval of information about their moisture levels using their reflectance profiles<sup>27–30</sup> is object of extensive research. Although their transmittance profiles are also affected by their water content<sup>8</sup> and have a direct influence on these soils' capability of eliciting seed germination and sustaining plant development,<sup>11,20,31,32</sup> works addressing these connections remain relatively meager in the related literature. The research described in this paper seeks to further the current understanding about the sensitivity of sand-textured soils' LPD to distinct patterns of water presence.

In order to achieve this goal without being constrained by laboratory and logistics limitations, we performed an array of controlled computational (*in silico*) experiments to systematically evaluate the effects of distinct water saturation states on the light penetration depths of representative samples of natural sands. The simulation of these states accounted for the presence of water both in the sample's pore space and forming encapsulating films around their grains. Our investigation was centered at the 400 to 1000 *nm* spectral domain, which is often employed in the analysis of these soils' mineralogy<sup>33–36</sup> and the study of related biophysical processes.<sup>8,11,37,38</sup>

To carry out our *in silico* experiments, we employed a first-principles simulation framework that comprehensively takes into account the mineralogy, granular structure and morphology of sand-textured soils. This investigation approach supported by actual measured data enabled us to obtain high-fidelity quantitative and qualitative depictions of the interplay between water presence and light penetration in these ubiquitous granular materials. Accordingly, our findings are expected to strengthen the knowledge base required for the development of new technologies aimed at the cost-effective monitoring and management of landscapes covered by natural sand deposits, as well as at the acquisition of more precise data related to fundamental photobiological phenomena (*e.g.*, seed germination<sup>10</sup> and pesticide degradation<sup>12</sup>) with a direct impact on crop yield and the recovery of ecosystems affected by the expansion of arid terrains.

The remainder of this paper is organized as follows. In Section 2, we provide an overview of relevant mineralogical and morphological characteristics of sand-textured soils. In Section 3, we describe our investigation framework. In Section 4, we present our findings and discuss their practical implications. Finally, in Section 5, we conclude the paper and outline directions for future research.

## 2. OVERVIEW OF RELEVANT CHARACTERISTICS OF SAND-TEXTURED SOILS

Soils are primarily composed of grains (particles) of weathered rocks immersed in a medium of air and water (the pore space).<sup>39</sup> The fraction of the total volume of a soil sample not occupied by its constituent grains is

defined as its porosity.<sup>40</sup> This quantity, in turn, is tied to the soil texture, *i.e.*, the proportion of sand-sized grains (particles with dimensions between 0.05 to 2.0 *mm*), silt-sized grains (particles with dimensions between 0.002 to 0.05 *mm*) and clay-sized grains (particles with dimensions smaller than 0.002 *mm*) forming a soil sample,<sup>31,41</sup> with coarse soils normally being less porous than finer soils.<sup>40</sup> On average, naturally-occurring sand-textured soils contain at least 85% sand-sized particles,<sup>41</sup> and their porosity normally varies between 35 and 50%.<sup>39,42</sup>

The rocks forming the core (parent) material of the sand-textured soils' constituent grains are typically silicate minerals like quartz.<sup>43</sup> Trace amounts of mineral impurities, notably iron oxides (*e.g.*, hematite, goethite and magnetite), can significantly affect the spectral signatures of these soils,<sup>21,44</sup> particularly in the spectral region from 400 to 1000 *nm*. In fact, these impurities are largely responsible for these soils' color,<sup>45-47</sup> which can be used in the inference of their chemical and physical properties.<sup>34-36</sup>

The weathering processes responsible for the formation of sand-textured soils can affect the morphology of their constituent grains. For instance, the transportation of grains by wind may involve rolling, suspension and saltation processes<sup>48</sup> that can alter their roundness and sphericity.<sup>49</sup> While a high roundness value corresponds to smooth grain, a high sphericity value indicates a grain with a geometry close to that of a sphere.

The grains' core materials may occur as pure particles,<sup>50</sup> as particles mixed with impurities<sup>46</sup> or as coated particles.<sup>51</sup> A particle coating is formed by a mineral (*e.g.*, kaolinite) matrix that may embed impurities as a result of weathering processes as well.<sup>51</sup> We note that the iron oxides may also be present in a soil sample as pure particles.<sup>50</sup>

The presence of water in the pore space of a natural sand sample can be quantified in terms of its degree of water saturation, denoted by *S*. This quantity corresponds to the probability of light encountering water while traversing the pore space of a given sand sample,<sup>25</sup> and it can vary from zero (dry state) to one (water-saturated state).

There are also situations in which the grains of dry layers of natural sands, albeit immersed in a pore space filled with air, may be encapsulated by water films.<sup>24</sup> This may happen, for example, after the bulk of water in the pore space has been either drained via gravity or partially evaporated, leaving only the water films created by surface tension between the water and the grains.<sup>31</sup>

### 3. INVESTIGATION FRAMEWORK

#### 3.1 Selected Sand-Textured Soil Samples

In our investigation, we considered samples from four natural sand deposits with distinct morphological and mineralogical characteristics, namely a red (hematite-rich) Australian dune, a dark (magnetite-rich) Peruvian beach, a yellowish (goethite-rich) Californian outcrop and a red Saudi Arabian dune. We note that these samples were used in actual reflectance measurements performed by Rinker *et al.*<sup>52</sup>, whose results (made available in the U.S. Army Topographic Engineering Center database<sup>52</sup>) were employed as references (Section 3.3) in our investigation.

In the absence of complete characterization datasets for the selected samples (Rinker *et al.*<sup>52</sup> provided only their general descriptions), the values assigned to their parameters were chosen from physically valid ranges reported in the related literature<sup>25</sup> so that we could establish sound baselines (Section 3.3) for our *in silico* experiments. More specifically, in the characterization of the selected samples, we considered quartz as their core material and kaolinite as their coating matrix. In addition, we employed mean values for their porosity (0.425),<sup>39</sup> grain roundness (0.482)<sup>53</sup> and grain sphericity (0.798).<sup>53</sup> The remaining parameter values used in their characterization are given in Table 1.

The percentages of the sand-sized and silt-sized particles depicted in Table 1 are employed to compute the dimensions of the samples' grains using a particle size distribution provided by Shirazi *et al.*,<sup>54</sup> with average dimension values provided in (Table 2) for reference. Also, based on the samples' descriptions,<sup>52</sup> we assumed the presence of clay-sized particles to be negligible.

Samples	$s_a$	$s_i$	$\mu_p$	$\mu_m$	$\mu_c$	$r_{hg}$	$\vartheta_{hg}$	$\vartheta_m$
Australian dune	90	10	0	50	50	0.80	0.012	0.0
Peruvian beach	95	5	50	0	50	0.375	0.05	0.17
Californian outcrop	92.5	7.5	50	25	25	0.25	0.042	0.0
Saudi Arabian dune	90	10	0	75	25	0.5	0.012	0.0

Table 1: Parameter values used to characterize the sand-textured soil samples considered in this investigation. The texture of the samples is described by the percentages (%) of sand ( $s_a$ ) and silt ( $s_i$ ). The particle type distributions considered in the simulations are given in terms of the percentages (%) of pure ( $\mu_p$ ), mixed ( $\mu_m$ ) and coated ( $\mu_c$ ) grains. The parameter  $r_{hg}$  corresponds to the ratio between the mass fraction of hematite to  $\vartheta_{hg}$  (the total mass fraction of hematite and goethite). The parameter  $\vartheta_m$  represents the mass fraction of magnetite, which is assumed to appear as pure particles.<sup>55</sup>

Samples	$m_a$	$m_i$
Australian dune	0.126	0.022
Peruvian beach	0.141	0.021
Californian outcrop	0.132	0.022
Saudi Arabian dune	0.126	0.022

Table 2: Average dimensions (given in  $mm$ ) of the major axes  $m_a$  and  $m_i$  that respectively define the ellipsoids used to represent the sand-sized and the silt-sized particles forming the sand-textured soil samples considered in this investigation.

It is worth mentioning that Rinker *et al.*<sup>52</sup> did not report any presence of water or moisture when they performed the actual reflectance measurements employed as baseline references in this investigation. Accordingly, we set the samples' degree of water saturation to zero during the computation of the modeled reflectance curves presented in Section 3.3.

### 3.2 *In silico* Experimental Setup

During our controlled *in silico* experiments, we computed directional-hemispherical reflectance and transmittance curves using an enhanced implementation of the first-principles light transport model originally known as SPLITS (*Spectral Light Transport Model for Sand*).<sup>25</sup> The stochastic formulation employed by this model includes parameters describing the morphology and mineralogy of the particles forming sand-textured soils, as well as the distribution of these particles within the pore space. To enable the reproduction and extension of our *in silico* experimental results, we have made an enhanced implementation of SPLITS, termed SPLITS-2,<sup>56</sup> available online,<sup>57</sup> via a model distribution system,<sup>58</sup> along with the supporting spectral datasets (*e.g.*, refractive index and extinction coefficient curves<sup>59</sup>) associated with the various minerals considered in this investigation.

Each modeled radiometric curve was obtained using a virtual spectrophotometer<sup>60</sup> and casting  $10^6$  rays (per sampled wavelength) onto the natural sand samples. For the baseline reflectance experiments (Section 3.3), we considered the samples' thickness equal to  $1\ m$ , a default value that guarantees depth-invariant readings<sup>12</sup> like those obtained in the actual measurements.<sup>52</sup> For the transmittance experiments, we considered distinct values for the samples' thickness ( $1.0$ ,  $1.1$  and  $1.2\ mm$ ) to evaluate their light transmission profiles as described below. Furthermore, to increase our scope of observations, our experiments were carried out employing two distinct angles of light incidence ( $0^\circ$  and  $45^\circ$ ).

We considered four water saturation states (depicted in Fig. 1), henceforth referred to as States I, II, III and IV, in our *in silico* transmittance experiments: a dry state ( $S = 0$ ), an intermediate water-saturated state ( $S = 0.5$ ), a water-saturated state ( $S = 1$ ) and a dry state ( $S = 0$ ) with the grains encapsulated by water films, respectively. It is worth mentioning that the thickness of a water film depends on the sand sample's morphological characteristics, its previous water saturation state<sup>31,61</sup> and environmental factors such as temperature.<sup>62</sup> For the purposes of our investigation, we assigned to the water film thickness a value of  $5\ \mu m$ , which is consistent

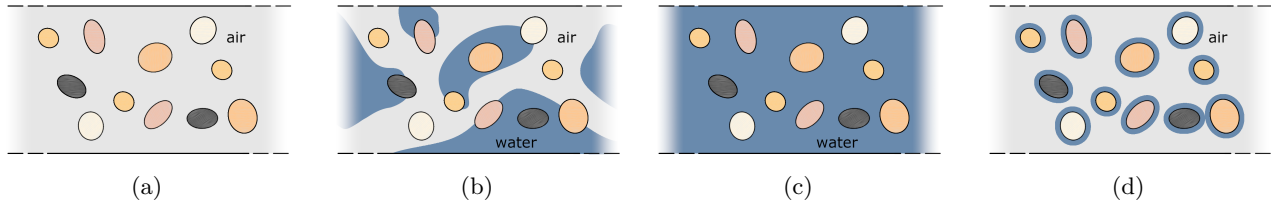


Figure 1: Diagrams (not to scale) illustrating the distinct water saturation states (associated with the presence, or absence, of water in the pore space of a given natural sand sample) considered in this investigation. For clarity purposes, only a relatively small number of grains (particles) are depicted in the diagrams. From (a) to (d), dry state, intermediate water-saturated state, water-saturated state and dry state with the grains encapsulated by water films, respectively.

with actual experiments involving the presence of water films encapsulating the grains of quartz-sand samples.<sup>61</sup>

In order to estimate the LPD ranges for the selected samples for each water saturation state, we computed transmittance curves for the samples considering different values for their thickness. We varied these thickness values in increments of  $0.1\text{ mm}$ , which corresponds to the precision of light penetration depths provided for sand-textured soils in the related literature.<sup>8,9</sup> The lower and upper limits of an estimated range are represented by the thickness values resulting in transmittance readings (in the  $400$  to  $1000\text{ nm}$  spectral domain) below and above  $1\%$ , respectively. These limits were then reported (Section 4) as the LPD ranges for the selected sample under the distinct *in silico* experimental conditions.

### 3.3 Baseline Experiments

We remark that the values assigned to the selected samples' characterization parameters were chosen based on the samples' general descriptions<sup>52</sup> and physically valid ranges reported for these parameters in the related literature. Thus, to assess the plausibility of our choice of parameter values, we computed reflectance curves using SPLITS-2 and compared them with the reflectance curves measured for the selected samples.<sup>52</sup> As it can be observed in Fig. 2, the modeled curves show a close agreement with their measured counterparts. Hence, unless otherwise stated, we employed the same parameter values in our *in silico* transmittance experiments.

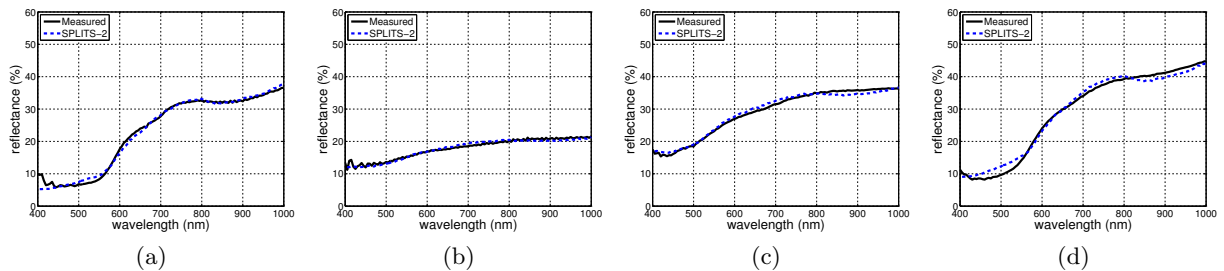


Figure 2: Comparisons of measured<sup>52</sup> and modeled (using SPLITS-2) reflectance curves obtained for the selected natural sand samples. From (a) to (d), Australian dune, Peruvian beach, Californian outcrop and Saudi Arabian dune samples, respectively. The modeled curves were computed considering an angle of incidence of  $0^\circ$  for consistency with the actual experimental setup<sup>25,52</sup> used to obtain the measured curves. From (a) to (d), the root mean square errors<sup>56</sup> computed for the modeled curves with respect to their measured counterparts were:  $0.0068$ ,  $0.0095$ ,  $0.0076$  and  $0.0132$ , respectively.

## 4. RESULTS AND DISCUSSION

Initially, to assess the fidelity of our *in silico* transmittance experiments, we compared the transmittance profiles obtained for the selected samples considering the four distinct water saturation states. These profiles, which are presented in Figs. 3 to 6, depict similar qualitative trends for all four states. More specifically, one can observe an expected nonlinear decrease in transmittance following a linear increase in the samples' thickness, and a slight decrease in transmittance following an increase in the angle of incidence.<sup>23</sup> The presence of water, however, resulted in higher transmittance readings (presented in Figs. 4 to 5) in comparison with the readings (presented in Fig. 3) obtained for the samples in the dry state. This behaviour is consistent with actual experimental observations<sup>8,20,63</sup> on the transmittance of wet sand-textured soils.

It has been observed that an intermediate state of water saturation ( $S = 0.5$ ) approximately corresponds to the field capacity of a soil, *i.e.*, the amount of water available for plant uptake until the permanent wilting point is reached.<sup>31</sup> This point, in turn, corresponds to the stage in which the water is held too firmly by the soil grains (forming the encapsulating films around them) for plants to extract it.<sup>31</sup> By examining the graphs depicted in Figs. 4 and 6, one can note that the results obtained for State II were not only qualitatively, but also quantitatively similar to those obtained for State IV. This suggests that, from a light transmission perspective, when a sand-textured soils reaches its field capacity, the resulting impact on its LPD tends to be the same as that observed when it reaches its permanent wilting point.

We then proceeded to compute the LPD ranges for the selected samples considering the spectral region of interest (from 400 to 1000 *nm*). The obtained values are provided in Tables 3 and 4. For the samples in a dry state (Table 3), a thickness between 1.2 to 1.3 *mm* was required to obtain transmittance values below 1% in the worst case (Saudi Arabian dune sample). We remark that the literature on this topic is scant, particularly with respect to actual measured data, and direct comparisons are difficult to be performed in view of the limited descriptions of the samples used in the actual experiments. Nonetheless, our estimated ranges are consistent with values provided in related works. For instance, Woolley and Stoller<sup>8</sup> reported transmittance values (from 350 to 800 *nm*) below 2% for a depth of 1.1 *mm* in a dry natural sand sample. Also, Benvenuti<sup>9</sup> reported a light penetration depth of 1 *mm* in his experiments (from 400 to 800 *nm*) on a dry sample with 93% of its granular structure composed of sand-sized particles.

For the *in silico* experimental instances in which we accounted for the presence of water in the samples' pore space, the computed ranges (Table 3) indicated an increase in the samples' light penetration depth following an increase in their degree of water saturation. In the worst case (water-saturated Saudi Arabian dune sample), a thickness between 2.2 to 2.3 *mm* was required to obtain transmittance values below 1%. Such an increase in the light penetration depth was to be expected in view of the increase in transmittance elicited by the presence of water.<sup>8,12</sup>

By examining the ranges presented in Table 3, one can also note that those computed considering the samples' grains encapsulated by water films (State IV) were similar to those computed considering the samples in an intermediate water-saturated state (State II). In the worst case (Saudi Arabian dune sample), a thickness between 1.5 and 1.6 *mm* was required to obtain transmittance values below 1%. We note that Woolley and Stoller<sup>8</sup> reported transmittance values (from 350 to 800 *nm*) below 1% for a depth of 2.2 *mm* in a moist sand sample composed of particles with a diameter between 0.3 to 0.5 *mm*. It has been noted that transmittance decreases following a reduction in the size of a sample's constituent grains.<sup>9,12,19</sup> Accordingly, for sand samples characterized by smaller particles, like those considered in this investigation (Table 2), one should expect a value for light penetration depth lower than that reported by Woolley and Stoller.<sup>8</sup>

Another aspect worth of stressing is the influence of the selected samples' mineralogy on their LPD ranges. As expected, the lowest ranges were obtained for the Peruvian sample which was characterized by the highest iron oxide contents. Although, the Australian and the Saudi Arabian samples were characterized by similar iron oxide contents, the distribution patterns of the mineral impurities within these samples were different. This resulted in markedly distinct LPD ranges for these samples. Conversely, even though the Australian and Californian samples were characterized by different iron oxide contents, they presented similar LPD ranges, which can also be attributed to their different iron oxide distribution patterns. This suggests that the LPD of natural sands is affected not only by their iron oxide contents, but also by the distribution patterns of these mineral impurities.

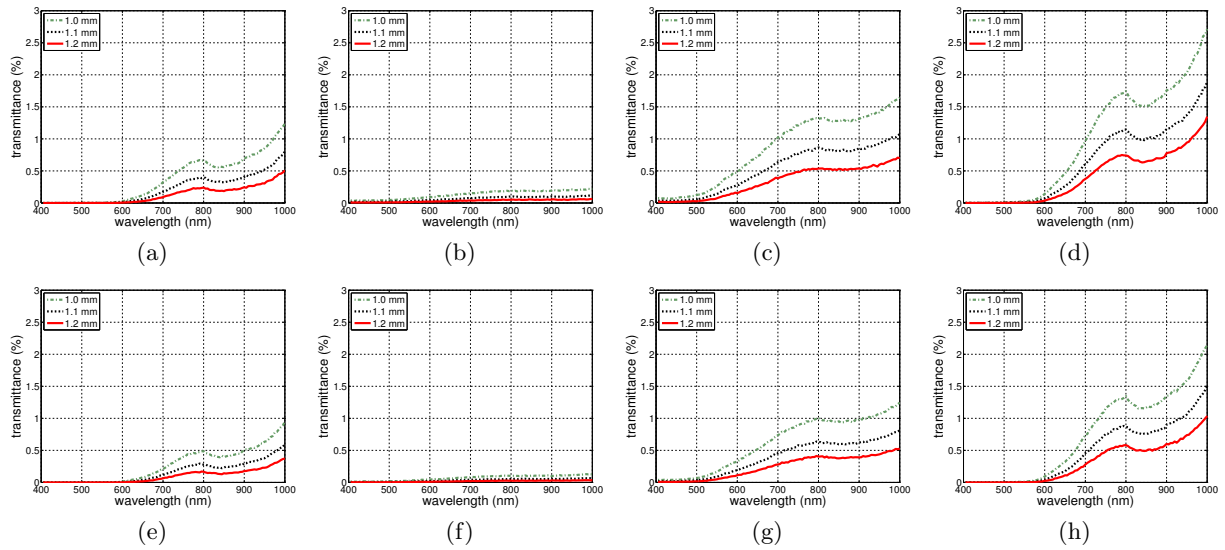


Figure 3: Comparisons of transmittance curves obtained for the selected sand-textured soil samples in a dry state ( $S = 0$ ). The curves were computed considering distinct values for their thickness (1.0, 1.1 and 1.2 mm). (a) and (e): Australian dune. (b) and (f): Peruvian beach. (c) and (g): Californian outcrop. (d) and (h): Saudi Arabian dune samples. Top row: angle of incidence of  $0^\circ$ . Bottom row: angle of incidence of  $45^\circ$ .

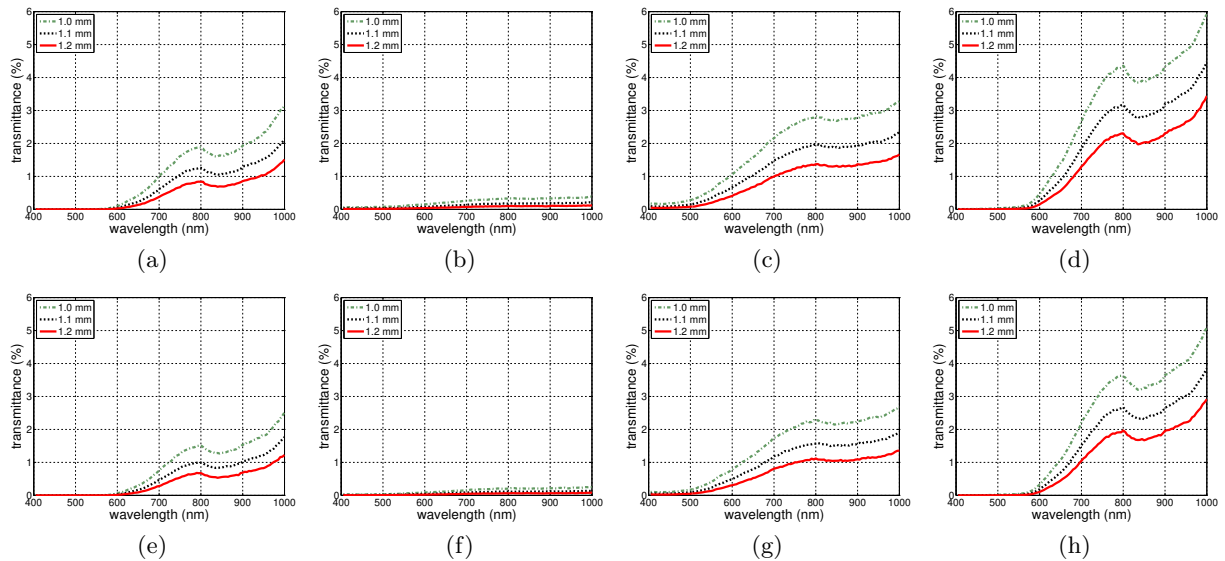


Figure 4: Comparisons of transmittance curves obtained for the selected sand-textured soil samples in an intermediate water-saturated state ( $S = 0.5$ ). The curves were computed considering distinct values for their thickness (1.0, 1.1 and 1.2 mm). (a) and (e): Australian dune. (b) and (f): Peruvian beach. (c) and (g): Californian outcrop. (d) and (h): Saudi Arabian dune samples. Top row: angle of incidence of  $0^\circ$ . Bottom row: angle of incidence of  $45^\circ$ .

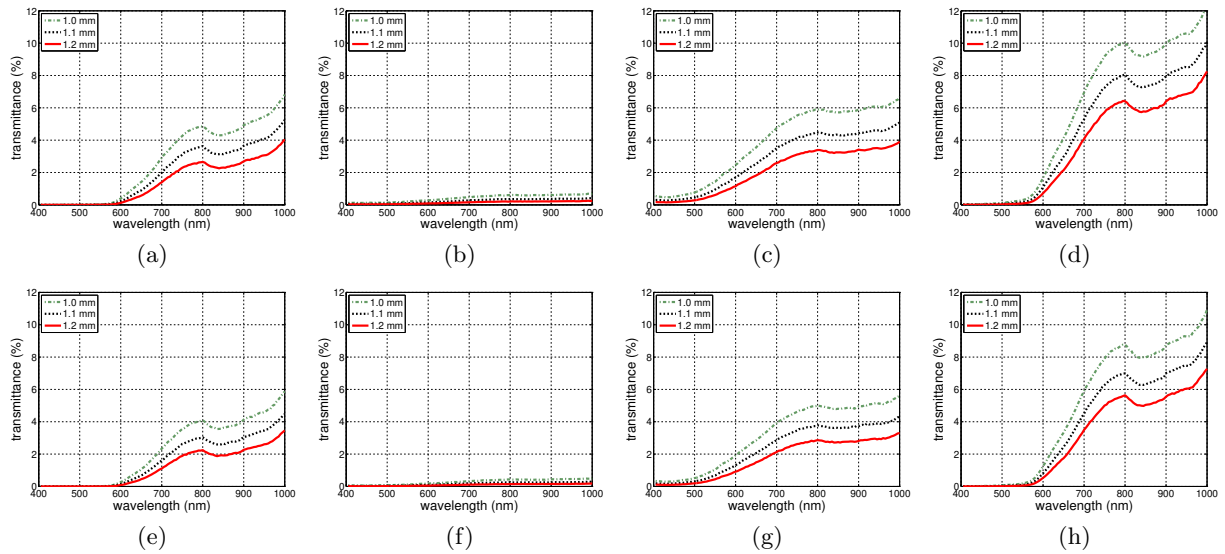


Figure 5: Comparisons of transmittance curves obtained for the selected sand-textured soil samples in a water-saturated state ( $S = 1$ ). The curves were computed considering distinct values for their thickness (1.0, 1.1 and 1.2 mm). (a) and (e): Australian dune. (b) and (f): Peruvian beach. (c) and (g): Californian outcrop. (d) and (h): Saudi Arabian dune samples. Top row: angle of incidence of  $0^\circ$ . Bottom row: angle of incidence of  $45^\circ$ .

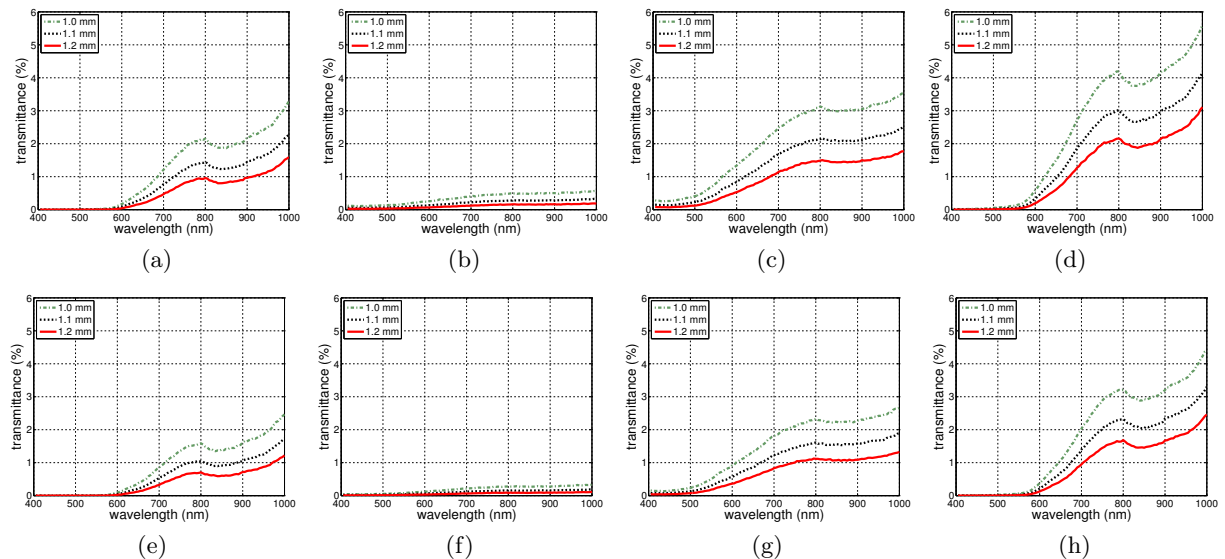


Figure 6: Comparisons of transmittance curves obtained for the selected sand-textured soil samples in a dry state ( $S = 0$ ) with the grains encapsulated by water films. The curves were computed considering distinct values for their thickness (1.0, 1.1 and 1.2 mm). (a) and (e): Australian dune. (b) and (f): Peruvian beach. (c) and (g): Californian outcrop. (d) and (h): Saudi Arabian dune samples. Top row: angle of incidence of  $0^\circ$ . Bottom row: angle of incidence of  $45^\circ$ .

Samples	Water Saturation States			
	I	II	III	IV
Australian dune	1.0 - 1.1	1.3 - 1.4	1.7 - 1.8	1.3 - 1.4
Peruvian beach	0.7 - 0.8	0.8 - 0.9	0.9 - 1.0	0.9 - 1.0
Californian outcrop	1.1 - 1.2	1.3 - 1.4	1.7 - 1.8	1.3 - 1.4
Saudi Arabian dune	1.2 - 1.3	1.6 - 1.7	2.2 - 2.3	1.5 - 1.6

Table 3: LPD ranges (in  $mm$ ) computed for the selected natural sand samples considering an angle of incidence of  $0^\circ$  and the values assigned to their iron oxide parameters ( $\vartheta_{hg}$  and  $\vartheta_m$ ) presented in Table 1. Specific ranges are presented for each water saturation state considered in this investigation: I - dry ( $S = 0$ ), II - intermediate ( $S = 0.5$ ), III - saturated ( $S = 1$ ), and IV - dry ( $S = 0$ , with the individual grains encapsulated by water films).

Samples	Water Saturation States			
	I	II	III	IV
Australian dune	0.9 - 1.0	1.2 - 1.3	1.6 - 1.7	1.2 - 1.3
Peruvian beach	0.6 - 0.7	0.7 - 0.8	0.8 - 0.9	0.8 - 0.9
Californian outcrop	1.0 - 1.1	1.2 - 1.3	1.6 - 1.7	1.2 - 1.3
Saudi Arabian dune	1.2 - 1.3	1.5 - 1.6	2.2 - 2.3	1.5 - 1.6

Table 4: LPD ranges (in  $mm$ ) computed for the selected natural sand samples considering an angle of incidence of  $45^\circ$  and the values assigned to their iron oxide parameters ( $\vartheta_{hg}$  and  $\vartheta_m$ ) presented in Table 1. Specific ranges are presented for each water saturation state considered in this investigation: I - dry ( $S = 0$ ), II - intermediate ( $S = 0.5$ ), III - saturated ( $S = 1$ ), and IV - dry ( $S = 0$ , with the individual grains encapsulated by water films).

When we considered an angle of incidence of  $45^\circ$ , the resulting LPD ranges, presented in Table 4, depicted the same qualitative trends observed for the LPD ranges obtained considering an angle of incidence of  $0^\circ$ , presented in Table 3. Quantitatively, the values obtained for the LPD ranges considering an angle of incidence of  $45^\circ$  were lower, which can be explained by the decrease of transmittance following an increase in the angle of incidence.<sup>23</sup>

To further extend our scope of observations, we also computed the LPD ranges considering a  $10\times$  reduction in the samples' iron oxide contents represented by the parameters  $\vartheta_{hg}$  and  $\vartheta_m$ . For conciseness, the corresponding transmittance curves are provided elsewhere.<sup>64</sup> The magnitude of the resulting LPD ranges, which are presented in Tables 5 and 6, was substantially higher than that of the ranges, presented in Tables 3 and 4, associated with the default values assigned to these parameters (Table 1). In the worst case for the samples in a dry state (Saudi Arabian dune sample), a thickness between 2.9 to 3.0  $mm$  was required to obtain transmittance values below 1%. Such higher values were expected due to an increase in transmittance following a substantial reduction in light attenuation associated with a reduced presence of iron oxides.<sup>9</sup> Also, as expected, the presence of water further increased the samples' light penetration depths. In the worst case (water-saturated Saudi Arabian dune sample), a thickness between 5.6 to 5.7  $mm$  was required to obtain transmittance values below 1%. We note, however, that the LPD trends associated with the samples' distinct patterns of iron oxide distribution observed in the values presented in Tables 3 and 4 are not observed in the values presented in Tables 5 and 6.

In short, by comparing the ranges presented in Tables 5 and 6 with their counterparts depicted in Tables 3 and 4, one can verify the importance of accounting for the fact that both the relatively small amounts of iron oxides found in natural sands and the distinct distribution patterns of these mineral impurities can have a significant influence on these soils' LPD ranges. Consequently, experiments employing samples with iron oxide contents and distribution patterns that are not normally found in natural sand deposits are inadequate to provide quantitative predictions about these soils. The technical inferences that one can obtain from such experiments tend to be more appropriate to support the analysis of qualitative aspects. For example, recent spectrophotometric measurements<sup>22</sup> performed on a coarse (85% of the particles with a diameter between 0.5 and 1  $mm$ ) "white" sand samples with insignificant iron oxide amounts resulted in an upper bound for transmittance values (in the 400 to 1000  $nm$  region) equal to 20% for a depth of 3  $mm$ . This bound was substantially increased when water was added to the samples, a behaviour qualitatively congruent with the trends observed in our *in silico* experiments.

Samples	Water Saturation States			
	I	II	III	IV
Australian dune	2.3 - 2.4	3.0 - 3.1	4.4 - 4.5	2.9 - 3.0
Peruvian beach	2.1 - 2.2	2.7 - 2.8	3.7 - 3.8	2.8 - 2.9
Californian outcrop	2.8 - 2.9	3.5 - 3.6	5.3 - 5.4	3.4 - 3.5
Saudi Arabian dune	2.9 - 3.0	3.7 - 3.8	5.6 - 5.7	3.4 - 3.5

Table 5: LPD ranges (in  $mm$ ) computed for the selected natural sand samples considering an angle of incidence of  $0^\circ$  and a  $10\times$  reduction in the values assigned to their iron oxide parameters ( $\vartheta_{hg}$  and  $\vartheta_m$ ) presented in Table 1. Specific ranges are presented for each water saturation state considered in this investigation: I - dry ( $S = 0$ ), II - intermediate ( $S = 0.5$ ), III - saturated ( $S = 1$ ), and IV - dry ( $S = 0$ , with the individual grains encapsulated by water films).

Samples	Water Saturation States			
	I	II	III	IV
Australian dune	2.2 - 2.3	3.0 - 3.1	4.4 - 4.5	2.8 - 2.9
Peruvian beach	2.0 - 2.1	2.6 - 2.7	3.6 - 3.7	2.7 - 2.8
Californian outcrop	2.6 - 2.7	3.4 - 3.5	5.2 - 5.3	3.3 - 3.4
Saudi Arabian dune	2.8 - 2.9	3.6 - 3.7	5.6 - 5.7	3.2 - 3.3

Table 6: LPD ranges (in  $mm$ ) computed for the selected natural sand samples considering an angle of incidence of  $45^\circ$  and a  $10\times$  reduction in the values assigned to their iron oxide parameters ( $\vartheta_{hg}$  and  $\vartheta_m$ ) presented in Table 1. Specific ranges are presented for each water saturation state considered in this investigation: I - dry ( $S = 0$ ), II - intermediate ( $S = 0.5$ ), III - saturated ( $S = 1$ ), and IV - dry ( $S = 0$ , with the individual grains encapsulated by water films).

We remark that the understanding and quantification of light penetration in sand-textured soils is essential for the successful use of hyperspectral technologies, both remotely and *in situ*, to tackle practical problems in various fields. These include, for example, the restoration of vegetation in desertified areas, weed control in arable terrains and the detection of signatures of subsurface targets in sandy landscapes. The presence of water increases light penetration through sand-textured soils. Among a number of photobiological phenomena, this affects the germination of photoblastic seeds, which depends on the amount of light reaching them, particularly during long exposure periods.<sup>10</sup> Although water is usually scant in arid regions, our findings indicate that its presence forming thin films around the grains of otherwise dry sand-textured soils (State IV) can increase light penetration by the same amount that would be verified should these soils reach their field capacity (State II). Thus, the presence of water films not only increases the probability of eliciting photoblastic seed germination in these soils, but also facilitates the identification of subsurface targets. Our findings also show that the magnitude of the impact of distinct water saturation states on light penetration can vary significantly depending on the mineralogical and morphological characteristics of natural sands. Hence, by overlooking the relatively small, but pivotal, presence of iron oxides and their different distribution patterns in these soils, one can hinder the fidelity of estimations of their LPD. This, in turn, is likely to be detrimental to the effectiveness of the applications mentioned above.

## 5. CONCLUSION AND PERSPECTIVES

In this paper, we have investigated the impact of distinct water saturations states on the light penetration depth of sand-textured soils. Using a first-principles *in silico* investigation framework, we were able to overcome technological constraints in order to conduct a series of controlled transmittance experiments on representative samples of these soils. The outcomes of our *in silico* experiments, albeit still subject to *in situ* verification, provide a detailed evaluation of variations on their LPD in response to changes in water saturation conditions.

As future work, we plan to extend our research to other soil types, notably clay-textured soils, as more supporting material characterization data become available. Besides the macropores found in sand-textured

soils, clayey soils also have micropores within peds formed by the aggregation of clay particles and the adhesion of iron oxides and other substances (*e.g.*, carbonates).<sup>31</sup> The combined effects of water and iron oxides on the penetration of light in soils with these morphological arrangements is likely to be quantitatively and qualitatively distinct from those verified in sand-textured soils. We intend to include the examination of this hypothesis in our agenda of subsequent investigations in this area.

It is also worth noting that organic matter, or humus, can be found in relatively small amounts in sand-textured soils found in certain landscapes.<sup>39</sup> This black substance, composed of animal and/or plant remains,<sup>39</sup> is characterized by strong light attenuation properties. Accordingly, despite its relatively low concentration ( $\approx 2\%$ ) in these soils, it can result in a significant masking of iron oxides' effects on their spectral responses.<sup>65</sup> Similarly, salts found in natural sands covering arid and semiarid landscapes (where evaporation exceeds precipitation<sup>31</sup>) can also affect the spectral responses of these soils.<sup>66</sup> Again, as more supporting radiometric data for these substances becomes available, the investigation of their effects on the light penetration depth of natural sands would also represent another relevant topic for future research in this area.

Finally, it is important to underline the fact only a relatively small number of works aimed at the study of light penetration in natural sands can be found in the related literature. The improvement of this situation can bring benefits to various disciplines. Accordingly, the scientific community needs to provide a continuing support for efforts involving the measurement of these soils' radiometric properties (reflectance and transmittance) and the acquisition of reliable hyperspectral data (*e.g.*, extinction coefficients and refractive indices) for their constituent materials. Moreover, it should also foment the pairing of these efforts with the use of simulation frameworks that can predictively reproduce their spectral responses to a wide scope of environmental stimuli. We believe that these synergistic collaborations can be instrumental to the achievement of robust advances in applications involving light interactions with different types of soils.

## ACKNOWLEDGMENTS

This work was supported by the Natural Sciences and Engineering Research Council of Canada (NSERC-Discovery Grant 238337).

## REFERENCES

- [1] Cooke, R. and Warren, A., [*Geomorphology in Deserts*], University of California Press, Los Angeles, CA, USA (1973).
- [2] Yan, C., Wang, T., Han, Z., and Qie, Y., "Surveying sandy deserts and desertified lands in north-western China by remote sensing," *Int. J. Remote Sens.* **28**(16), 3603–3618 (2007).
- [3] Berdugo, M., Delgado-Baquerizo, M., Soliveres, S., Hernández-Clemente, R., Zhao, Y., Gaitán, J., Gross, N., Saiz, H., Maire, V., Lehmann, A., Rillig, M., Solé, R., and Maestre, F., "Global ecosystem thresholds driven by aridity," *Science* **367**, 787–790 (2020).
- [4] Lai, L., Chen, L., Jiang, L., Zhou, J., Zheng, Y., and Shimizu, H., "Seed germination of seven desert plants and implications for vegetation restoration," *AoB Plants* **8**, 1–10 (2016).
- [5] Mula, D., "Twenty five years of remote sensing in precision agriculture: Key advances and remaining knowledge gaps," *Biosyst. Eng.* **114**, 358–371 (2013).
- [6] Akhlaq, M., Sheltami, T., and Mouftah, H., "A review of techniques and technologies for sand and dust storm detection," *Rev. Environ. Sci. Biotechnol.* **11**, 305–322 (2012).
- [7] Lambert, A., Hallar, A., Garcia, M., Strong, C., Andrews, E., and Hand, J., "Dust impacts of rapid agricultural expansion on the great plains," *Geophys. Res. Lett.* **47**(20), 1–11 (2020).
- [8] Woolley, J. and Stoller, E., "Light penetration and light-induced seed germination in soil," *Plant Physiol.* **61**, 597–600 (1978).
- [9] Benvenuti, S., "Soil light penetration and dormancy of Jimsonweed (*Datura stramonium*) seeds," *Weed Sci.* **43**, 389–393 (1995).
- [10] Pons, T., "Seed responses to light," in [*Seeds: The Ecology of Regeneration in Plant Communities*], Fenner, M., ed., 237–260, CABI Publishing, Wallingford, UK (2000).

- [11] Baranoski, G., Kimmel, B., Varsa, P., and Iwanchyshyn, M., “Porosity effects on the red to far-red ratios of light transmitted in natural sands: implications for photoblastic seed germination,” in [*Proc. of SPIE, Vol. 11149, Remote Sensing for Agriculture, Ecosystems, and Hydrology XXI, SPIE Remote Sensing*], Neale, C. and Maltese, A., eds., 111490O–1–14 (2019).
- [12] Ciani, A., Goss, K., and Schwarzenbach, R., “Light penetration in soil and particulate materials,” *Eur. J. Soil. Sci.* **56**, 561–574 (2005).
- [13] Huang, M., Chao, M. K. K., Qin, J., Mo, C., Esquerre, C., Delwiche, S., and Zhu, Q., “Penetration depth measurement of near-infrared hyperspectral imaging light for milk powder,” *Sensors* **441**(16), 1–11 (2016).
- [14] Lian, O., Huntley, D., and Wolfe, S., “Optical dating of eolian dune sand from Canadian prairies,” *Geogr. Phys. Quatern.* **56**(2-3), 191–202 (2002).
- [15] Ollerhead, J., “Light transmittance through dry, sieved sand: some test results,” *Ancient TL* **19**(1), 13–17 (2001).
- [16] Dickinson, W. and Ward, J., “Low depositional porosity in eolian sands and sandstones, Namib desert,” *J. Sediment. Res.* **A64**(2), 226–232 (1994).
- [17] Tang, D., Briggs, K., Williams, K., Jackson, D., Thorsos, E., and Percival, D., “Fine-scale volume heterogeneity measurements in sand,” *Soil Sci. Soc. Am. J.* **27**(3), 546–560 (2002).
- [18] Curry, C., Bennett, R., Hulbert, M., Curry, K., and Faas, R., “Comparative study of sand porosity and a technique for determining porosity of undisturbed marine segment,” *Mar. Georesour. Geotec.* **22**, 231–252 (2004).
- [19] Bänninger, D. and Flüehler, H., “Modeling light scattering at soil surfaces,” *IEEE T. Geosci. Remote* **42**(7), 1462–1471 (2004).
- [20] Tester, M. and Morris, C., “The penetration of light through soil,” *Plant Cell Environ.* **10**, 281 (1987).
- [21] Viallefont-Robinet, F., Bacour, C., Bouvet, M., Kheireddine, M., Ouhssain, M., Idoughi, R., Grignon, L., Munesa, E., Lemaître, F., and Rivière, T., “Contributions to sandy site characterization: spectro-directional signature, grain size distribution and mineralogy extracted from sand samples,” *Remote Sens.* **11**(2446), 1–24 (2019).
- [22] Tian, J. and Philpot, W., “Spectral transmittance of a translucent sand with directional illumination,” *IEEE T. Geosci. Remote* **56**(8), 4307–4317 (2018).
- [23] Baranoski, G., Kimmel, B., Varsa, P., and Iwanchyshyn, M., “On the light penetration in natural sands,” in [*International Geoscience and Remote Sensing Symposium - IGARSS 2019*], 6933–6936, IEEE (2019).
- [24] Neema, D., Shah, A., and Patel, A., “A statistical model for light reflection and penetration through sand,” *Int. J. Remote Sens.* **8**(8), 1209–1217 (1987).
- [25] Kimmel, B. and Baranoski, G., “A novel approach for simulating light interaction with particulate materials: application to the modeling of sand spectral properties,” *Opt. Express* **15**(15), 9755–9777 (2007).
- [26] Kimmel, B. and Baranoski, G., “Simulating the appearance of sandy landscapes,” *Comput. Graph.* **34**(4), 441–448 (2010).
- [27] Shuman, R., “Determination of beach sand parameters using remotely sensed aircraft reflectance data,” *Remote Sens. Environ.* **11**, 295–310 (1981).
- [28] Nolet, C., Poortings, A., Roosjen, P., Bartholomeus, H., and Ruessink, G., “Measuring and modeling the effect of surface moisture on the spectral reflectance of coastal beach sand,” *PLOS One* **9**(1), e112151:1–9 (2014).
- [29] Baranoski, G. and Kimmel, B., “Can porosity affect the hyperspectral signature of sandy landscapes?,” in [*Proc. of SPIE, Vol. 10428, Earth Resources and Environmental Remote Sensing/GIS Applications VIII SPIE, Remote Sensing*], Michel, U. and Schulz, K., eds., 104280S1–7 (2017).
- [30] Bablet, A., Viallefont-Robinet, F., Jacquemoud, S., Fabre, S., and Briottet, X., “High-resolution mapping of in-depth soil moisture content through a laboratory experiment coupling a spectroradiometer and two hyperspectral cameras,” *Remote Sens. Environ.* **236**, 111533:1–11 (2020).
- [31] McCauley, A., Jones, C., and Jacobsen, J., “Basic soil properties,” Tech. Rep. Soil & Water, Management Module I, Montana State University, USA (2005).
- [32] Bejarano, M., Villar, R., Murillo, A., and Quero, J., “Effects of soil compaction and light on the growth of *Quercus pyrenaica* Willd. (*Fagaceae*) seedlings,” *Soil Till Res.* **110**, 108–114 (2010).

- [33] Manchanda, M., Kudrat, M., and Tiwari, A., “Soil survey and mapping using remote sensing,” *Trop. Ecol.* **43**(1), 61–74 (2002).
- [34] Levin, N., Ben-Dor, E., and Singer, A., “A digital camera as a tool to measure colour indices and related properties of sandy soils in semi-arid environments,” *Int. J. Remote Sens.* **26**(24), 5475–5492 (2005).
- [35] Rossel, R., Bui, E., de Caritat, P., and McKenzie, N., “Mapping iron oxides and the color of Australian soil using visible-near-infrared reflectance spectra,” *J. Geophys. Res.* **115**, F04031:1–3 (2010).
- [36] Adnani, M., Azzaoui1, M., Elbelrhiti, H., Ahmamou, M., Masmoudi, L., and Chiban, M., “Yerdi sand dunes (Erfoud area, southeastern of Morocco): color, composition, sand’s provenance, and transport pathways,” *Arab J. Geosci.* **9**(366), 1–15 (2016).
- [37] Kasperbauer, M. and Hunt, P., “Biological and photometric measurement of light transmission through soils of various colors,” *Bot. Gaz.* **149**(4), 361–364 (1988).
- [38] Bliss, D. and Smith, H., “Penetration of light into soil and its role in the control of seed germination,” *Plant Cell Environ.* **8**, 475–483 (1985).
- [39] Brady, N., [*The Nature and Properties of Soils*], Macmillan Publishing Co., New York, NY, USA, 8th ed. (1974).
- [40] Brady, N. and Weil, R., [*Elements of the Nature and Properties of Soils*], Prentice-Hall Inc., Upper Saddle River, NJ, USA (2000).
- [41] Soil Sci. Division Staff, “Soil survey manual,” Tech. Rep. USDA Handbook 18, Soil Conservation Service, United States Department of Agriculture, USA (1993).
- [42] Román-Sierra, J., Muñoz-Perez, J., and Navarro-Plus, M., “Beach nourishment effects on sand porosity variability,” *Coast. Eng.* **83**, 221–232 (2014).
- [43] Leu, D., “Visible and near-infrared reflectance of beach sands: a study on the spectral reflectance/grain size relationship,” *Remote Sens. Environ.* **6**(3), 169–182 (1977).
- [44] Bullard, J. and White, K., “Quantifying iron oxide coatings on dune sands using spectrometric measurements: An example from the Simpson-Strzelecki desert, Australia,” *J. Geophys. Res.* **107**(B6), 1–11 (2002).
- [45] Cornell, R. and Schwertmann, U., [*The Iron Oxides*], Wiley-VCH GmbH & Co. KGaA, Weinheim, Germany, 2nd ed. (2003).
- [46] Mottana, A., Crespi, R., and Liborio, G., [*Simon and Schuster’s Guide to Rocks and Minerals*], Simon and Schuster, Inc., New York, NY, USA (1978).
- [47] Torrent, J., Schwertmann, U., Fetcher, H., and Alferez, F., “Quantitative relationships between soil color and hematite content,” *Soil Sci.* **136**, 354–356 (1983).
- [48] Wadell, H., “Volume, shape, and roundness of rock particles,” *J. Geol.* **40**(5), 443–451 (1932).
- [49] Wadell, H., “Sphericity and roundness of rock particles,” *J. Geol.* **41**(3), 310–331 (1933).
- [50] Catling, D. and Moore, J., “The nature of coarse-grained crystalline hematite and its implications for the early environment of Mars,” *Icarus* **165**, 277–300 (2003).
- [51] Wopfner, H. and Twidale, C., “Australian desert dunes: wind rift or depositional origin?,” *Aust. J. Earth Sci.* **48**, 239–244 (2001).
- [52] Rinker, J., Breed, C., McCauley, J., and Corl, P., “Remote sensing field guide – desert,” Tech. Rep. ETL-0588, U.S. Army Topographic Engineering Center, Fort Belvoir, VA, USA (September 1991).
- [53] Vepraskas, M. and Cassel, D., “Sphericity and roundness of sand in costal plain soils and relationships with soil physical properties,” *Soil Sci. Soc. Am. J.* **51**(5), 1108–1112 (1987).
- [54] Shirazi, M., Boersma, L., and Hart, J., “A unifying quantitative analysis of soil texture: Improvement of precision and extension of scale,” *Soil Sci. Soc. Am. J.* **52**(1), 181–190 (1988).
- [55] Baranoski, G., Chen, B. K. T., and Miranda, E., “Influence of sand-grain morphology and iron-oxide distribution patterns on the reflectance of sand-textured soils,” *IEEE J-STARS* **7**(9), 3755–3763 (2014).
- [56] Iwanchyshyn, M., Kimmel, B., and Baranoski, G., “Revisiting the SPLITS model: Towards an enhanced implementation,” Tech. Rep. CS-2020-01, D.R. Cheriton School of Computer Science, University of Waterloo, Canada (2020).
- [57] Natural Phenomena Simulation Group (NPSG), *Run SPLITS-2 Online*. D.R. Cheriton School of Computer Science, University of Waterloo, Ontario, Canada (2020). <http://www.npsg.uwaterloo.ca/models/splits2.php>.

- [58] Baranoski, G., Dimson, T., Chen, T., Kimmel, B., Yim, D., and Miranda, E., “Rapid dissemination of light transport models on the web,” *IEEE Comput. Graph.* **32**(3), 10–15 (2012).
- [59] Natural Phenomena Simulation Group (NPSG), *Sand Data*. D.R. Cheriton School of Computer Science, University of Waterloo, Ontario, Canada (2012). <http://www.npsg.uwaterloo.ca/data/sand.php>.
- [60] Baranoski, G., Rokne, J., and Xu, G., “Virtual spectrophotometric measurements for biologically and physically-based rendering,” *The Visual Comput.* **17**(8), 506–518 (2001).
- [61] Mekonen, A., Sharma, P., and Fagerlund, F., “Transport and mobilization of multiwall carbon nanotubes in quartz sand under varying saturation,” *Environ. Earth Sci.* **71**, 3751–3760 (2014).
- [62] Li, W., Zhang, Y., Wei, W., and Gu, Z., “Discussions of some issues for wind blown sand flow simulation,” *Procedia IUTAM* **17**, 1190128 (2015).
- [63] Mandoli, D., Ford, G., Waldron, L., Nemson, J., and Briggs, W., “Some spectral properties of several soil types: implications for photomorphogenesis,” *Plant Cell Environ.* **13**, 287–294 (1990).
- [64] Iwanchyshyn, M., *In Silico Investigation of the Light Transmission Profiles of Sand-Textured Soils*, Master’s thesis, D.R. Cheriton School of Computer Science, University of Waterloo, Canada (2020).
- [65] Baumgardner, M., Silva, L., Biehl, L., and Stoner, E., “Reflectance properties of soils,” *Adv. Agron.* **38**, 1–43 (1985).
- [66] Jina, P., Lib, P., Wang, Q., and Pu, Z., “Developing and applying novel spectral feature parameters for classifying soil salt types in arid land,” *Ecol. Indic.* **54**, 116–123 (2015).